

Suppressed Kondo screening in two-dimensional altermagnets

G. S. Diniz^{1,*} and E. Vernek^{2,3,†}

¹*Curso de Física, ICET, Universidade Federal de Jataí, Jataí, GO 75801-615, Brazil.*

²*Instituto de Física, Universidade Federal de Uberlândia, Uberlândia, MG 38400-902, Brazil*

³*Department of Physics, Zhejiang Normal University, Jinhua 321004, Zhejiang, P. R. China.‡*

(Dated: January 12, 2024)

We have studied the Kondo effect of a spin-1/2 impurity coupled to a two-dimensional altermagnet host material. To attain the low-temperature many-body Kondo physics of the system, we have performed a numerical renormalization group calculations that allows us to access the spectral properties of the system at zero temperature. The impurity spectral function and the Kondo temperature were calculated for different set of parameters, including Rashba spin-orbit coupling (RSOC) and an external magnetic field. Interestingly, in the RSOC and altermagnetic fields, the hybridization function is spin independent, despite the characteristic broken time-reversal symmetry (TRS) of the altermagnet. This is because the alternating sign of the spin splitting of the bands in the momentum space renders equal contributions for both spin components of the hybridization function. Our results demonstrate that, although the hybridization function is TR symmetric, the Kondo temperature is substantially suppressed by the altermagnet coupling. Moreover, we have investigated the effect of an external magnetic field applied in the altermagnet along different directions. Interestingly, we observe an important restraining of the Kondo peak which depends strongly on the direction of the field. This anisotropic effect is, however, masked if strong Zeeman splitting takes place at the impurity, as it shatter the Kondo-singlet state.

I. INTRODUCTION

Screening of localized magnetic moments by itinerant electrons in metallic systems is paradigmatic in many-body physics in condensed matter. This phenomenon, known as Kondo effect [1], is crucial for the understanding of both electronic transport and magnetic properties of metallic systems doped with magnetic atoms. The physical mechanism underlying this phenomenon was first proposed by J. Kondo in 1963 [2], as spin-flip scatterings of conduction electrons by magnetic impurities diluted in metallic systems, resulting in a minimal resistivity observed at low temperatures [3]. After more than fifty years of its discovery, Kondo effect has been studied in a variety of systems resulting in an abundance of scientific studies [4–7].

Since the Kondo effect results from an effective exchange interaction between the localized moments and itinerant electrons, individual characteristics of both may be equally important. Therefore, the conditions to which the conduction electrons are subject to may modify the screening of localized magnetic moments. For example, spin-polarized (ferromagnetic) bands are detrimental to Kondo screening because time reversal symmetry (TRS) — which is of key importance to spin-flip scattering process involved in the Kondo mechanism — is broken [8–10]. Another example is the electron-phonon interaction in the conduction band that results in a vanishing density of states of the conduction band at the

Fermi level and leading to rich Kondo screening phases. More recently, Kondo screening of magnetic impurities by spin-orbit coupled conduction electrons has been investigated [11, 12]. The fundamental question in this context is how spin-orbit coupling (SOC) modifies the Kondo temperature of the system [13].

Quite interestingly, although SOC produces important modification in the energy bands of the host materials, numerical renormalization analysis have shown that, at least in the high density regime, the effect is straightforward. The increase of SOC produce a small widening of the conduction band accompanied by a decreasing of the density of states at the Fermi level. Nonetheless, the effective hybridization between the impurity and the conduction electrons around the Fermi level decreases resulting in a decreasing of T_K [14]. It seems, therefore, that despite the fact that SOC produces spin-splitting in the energy bands, because TRS is preserved, it has a minor effect in the Kondo screening [15]. A natural follow up question one may ask is whether this is the case for any system with spin-splitting energy bands, for example, the recently discovered altermagnets [16, 17], with peculiar TRS broken energy bands.

Altermagnets are a newly investigated class of collinear two- and three-dimensional antiferromagnets that display a large broken spin degeneracy, even in the absence of SOC [17–19]. Since the very first reports on these materials, they are gaining considerable attention in the recent few years. Most of these studies focus on the peculiar properties featured by this emergent class of magnets materials, such as large anisotropic (non-relativistic and) spin-splitting in momentum space with protected symmetry points, accompanied by a zero (net) magnetization. This anisotropic spin-splitting leads to the prediction of remarkable physical properties such as gapless superconducting states with mirage gaps [20], “multi-piezo” effect

* e-mail: ginetom@gmail.com

† e-mail: vernek@ufu.br

‡ This work was concluded while visiting the Department of Physics, Zhejiang Normal University, Jinhua 321004, Zhejiang, P. R. China.

in V_2Se_2O monolayer [21], spin-polarized Andreev levels [22], Majorana zero modes with zero net magnetization [23], magnon bands with an alternating chirality splitting [24], among many others exotic properties.

In this paper, we study the Kondo screening of magnetic impurities in altermagnets. More specifically, we aim at investigating how the unusual magnetic properties of these materials modify the Kondo temperature of the system. To this end, we propose a spin-1/2 magnetic impurity coupled to an altermagnet host material described formally by a traditional single-impurity Anderson model (SIAM). To accomplish this, we employ the well-known numerical renormalization group (NRG) [25] that allows us to obtain the relevant low-temperature physical quantities. For instance, within NRG calculations we can obtain the local density of states LDOS at the impurity site, from which we estimate the Kondo temperature of the system. Our results shows that intriguing band structure of the altermagnets has interesting consequences on the Kondo physics: (i) despite the spin-split band due to broken TRS, there is no spin splitting in the impurity spectral function. This is because the integration of the self-energy over the entire Brillouin zone renders a spin-independent hybridization function. (ii) By comparing the effects of AM and RSOC to the Kondo temperature, we find that T_K is up to two order of magnitude smaller for AM coupling as compared to RSOC, for the *same strength*. (iii) In the presence of external magnetic field, \mathbf{B} , on the altermagnetic-magnetic impurity system, the suppression on the Kondo peak depends strongly on the direction of the applied field. This anisotropy is akin to what was obtained by one of us in quantum impurity coupled to SOC quantum wires [14].

The rest of this paper is structured as follows. In Sec. II we present the model Hamiltonian and the procedure to calculate the hybridization function. Section. III the NRG results are presented. We summarize and conclude in Sec. IV.

II. MODEL AND METHODS

A. Hamiltonian model

We consider a hybrid system composed by a spin-1/2 impurity coupled to a d-wave AM with RSOC, as illustrated in Fig. 1 (a). The total Hamiltonian of the system can be written in the form of a SIAM as,

$$H = H_0 + H_{\text{imp}} + H_{\text{hyb}}, \quad (1)$$

where H_0 , H_{imp} and H_{hyb} represents the host altermagnet material, the magnetic impurity and the coupling between electrons of the altermagnet and the magnetic impurity, respectively. More precisely, $H_0 = H_{\text{AM}} + H_{\text{RSOC}} + H_Z$, where H_{AM} describes, for instance, a d-wave altermagnet on a substrate [17, 19, 26]. H_{RSOC} accounts for the contribution of the Rashba SOC (RSOC) induced by an inversion asymmetry, which can naturally arise due to the substrate on which the AM is deposited.

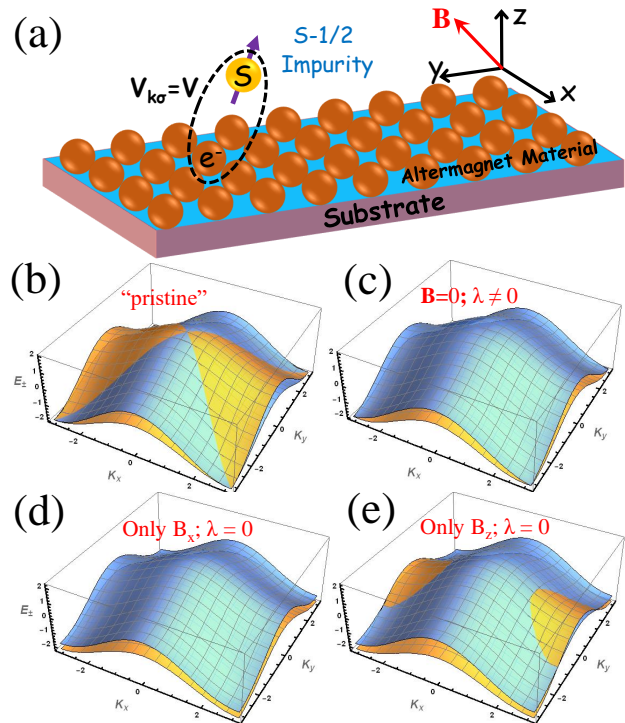


FIG. 1. (a) Schematic picture showing a spin-1/2 impurity coupled to an altermagnet material, which is deposited on a substrate and under an external magnetic field represented by the red arrow. (b) The $E_{\pm}(k_x, k_y)$ for *pristine* altermagnet (λ and \mathbf{B} are both zero) the zone boundary $-\pi/a \leq k_x(y) \leq \pi/a$. (c) $E_{\pm}(k_x, k_y)$ for the case when $\lambda \neq 0$ and $\mathbf{B} = 0$. (d) $E_{\pm}(k_x, k_y)$ for the case when $\lambda = 0$ and $\vec{B} = B\hat{x}$ (or $\mathbf{B} = B\hat{y}$ by symmetry). (e) Same as in (d), but for a magnetic field along the $\mathbf{B} = B\hat{z}$.

Finally, H_Z represents an external magnetic field. More explicitly, each of these terms are given by

$$\begin{aligned} H_{\text{AM}} &= 2t(\cos k_x + \cos k_y)\sigma_0 + 2t_{\text{AM}}(\cos k_x - \cos k_y)\sigma_z, \\ H_{\text{RSOC}} &= 2\lambda(\sin k_y\sigma_x - \sin k_x\sigma_y) = \mathbf{B}_{\text{SOC}}(\mathbf{k}) \cdot \boldsymbol{\sigma}, \quad (2) \\ H_Z &= g\mathbf{B} \cdot \mathbf{S}. \end{aligned}$$

Here, t the hopping amplitude parameter and t_{AM} stands for the AM exchange interaction. We have written H_{RSOC} as an effective k -dependent *magnetic field* $\mathbf{B}_{\text{SOC}}(\mathbf{k}) = 2\lambda(\sin k_y, -\sin k_x)$ is induced by the Rashba field, with λ standing for the strength of the interaction. The last term of Eq. (2), H_Z , describes the Zeeman effect in the AM material due to an external magnetic field \mathbf{B} , in which g is the effective g -factor of the AM. In all these terms, σ_i represents the Pauli matrices, including the identity σ_0 and $\mathbf{S} = \hbar\boldsymbol{\sigma}/2$.

The second term of the Eq. (1) is given by,

$$H_{\text{imp}} = \sum_{\sigma} \varepsilon_d n_{\sigma} + U n_{\uparrow} n_{\downarrow} + g_{\text{imp}} \mathbf{B} \cdot \mathbf{S}, \quad (3)$$

where, ε_d is the impurity on-site energy for spin σ (\uparrow or \downarrow), g_{imp} is the impurity g -factor, U represents the e - e interaction at the impurity site, and $n_{\sigma} = d_{\sigma}^{\dagger} d_{\sigma}$ is the electron number operator with spin σ .

Finally, the third term of Eq. (1) has the form

$$H_{\text{hyb}} = V \sum_{k\sigma} (d_{\sigma}^{\dagger} c_{k\sigma} + H.c.). \quad (4)$$

where we have assumed for simplicity, that the coupling strength between the impurity and the altermagnet is independent of momentum and spin component [27].

B. Energy band properties

The main features of the electronic bands given by Eq. 2 is shown in Fig. 1(b)-1(e), for different sets of parameter configurations. Fig. 1(b) shows the *pristine* case, which shows the alternating spin-splitting along the momentum and with degenerate points at Γ and also at the four corners of the Brillouin zone. In Fig. 1(c) we show the case where $\lambda \neq 0$ (while $\mathbf{B}=0$), which fully breaks the spin degeneracy of the bands, except at Γ points and at the four corners. In Fig. 1(d)-1(e) a \mathbf{B} is considered along different directions (with $\lambda=0$), where now there is no degeneracy at Γ and at the boundaries of the Brillouin zone. Below, we will return to the host band structure with a deeper analysis under different interactions.

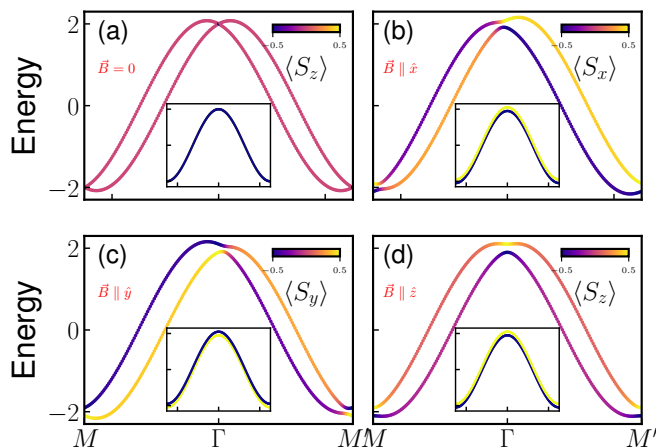


FIG. 2. Energy bands along the M - Γ - M' path for different parameters configurations: (a) $\mathbf{B} = 0$, (b) $\mathbf{B} = 0.05\hat{x}$, (c) $\mathbf{B} = 0.05\hat{y}$ and (d) $\mathbf{B} = 0.05\hat{z}$. For all panels, $t=0.5$, $t_{AM}=0.1$, $\lambda=0.2$, a Néel vector along the z -direction and the color map is associated to the spin-projection, $\langle S_i \rangle$, for each band. The insets correspond to each respective cases with $\lambda=0.0$.

Let us further analyze the host band structure in the presence of the external magnetic field. For the sake of numerical convenience, throughout the paper we will set, $g = k_B = 1.0 = \mu_B = \hbar = 1.0$. Fig. 2(a)-2(d) show the electronic band structure along the path M - Γ - M' , which is a good representative of the symmetries of the bands. In the absence of magnetic field and RSOC, the system shows an intriguing broken TRS with a momentum dependent alternating spin-splitting, as shown in Fig. 1(b). The band degeneracy along the path M - Γ - M' is broken

when RSOC is considered. However, they are still degenerated at the Γ and M (M') points, which is a consequence of the $C_{4z}\mathcal{T}$ symmetry that still holds [26]. This feature can be clearly seen in Fig. 2 (a), where we show the band structure for $\mathbf{B}=0$ and $\lambda = 0.2$ ($\lambda = 0.0$ for the inset). Moreover, the spin projection $\langle S_z \rangle$ is zero except at the spin-degenerate points, where the value is exactly $\langle S_z \rangle=0.5$ (and -0.5). Indeed, the spin projection would be non-zero (and equal, $\langle S_x \rangle=\langle S_y \rangle$) only along the plane $(x-y)$ (not shown in the panel). For an applied magnetic field in the plane x - y , say, at the x -(or y -direction), $C_{4z}\mathcal{T}$ -symmetry is broken as shown in Fig. 2(b)-2(c). We observe clear spin splittings of the bands at all points including Γ and M (M') which acquires a finite gap of $2g|\mathbf{B}|$, even for the $\lambda=0$ case (show in the insets). However, differently from the $\lambda=0$, the presence of RSOC induces a spin mixing of the bands with a broken inversion symmetry along M - Γ and Γ - M' path. Moreover, by alternating the direction of the in-plane \mathbf{B} field, the band structure around Γ point is reversed, with significant changes in the spin projection along the direction of the applied \mathbf{B} for $\lambda \neq 0$, with spin projections inverted at the Γ and M (M') points. At last, in Fig. 2(d) we show the case when \mathbf{B} is applied along the z -direction. As previously observed, the system is TRS-broken with a clear spin splitting. However, differently from the in-plane case, the system still has a symmetry along the cut line M - Γ - M' . From these results, we can confirm that the interplay between RSOC and magnetic field introduces important modifications to the altermagnet electronic bands, with a relevant anisotropy that can be crucial for the Kondo physics, as it will be further explored in the following sections.

C. Hybridization Function

The hybridization function of the impurity is of key importance in the NRG approach to the Kondo impurity problem. To obtain it, we first calculate the local impurity Green's function $\mathbf{G}_{\text{imp}}(\omega)$, which is a 2×2 matrix and can be written as [14, 28],

$$\mathbf{G}_{\text{imp}}(\omega) = \left[(\varepsilon_d - \omega)\sigma_0 - \boldsymbol{\Sigma}^{(0)}(\omega) - \boldsymbol{\Sigma}^{(\text{int})}(\omega) \right]^{-1}. \quad (5)$$

Here, $\boldsymbol{\Sigma}^{(0)}(\omega) = \sum_k \mathbf{V} \mathbf{G}_{\text{host}}(\mathbf{k}, \omega) \mathbf{V}^\dagger$ represents the non-interacting self-energy [28], with $\hat{V} = V\sigma_0$ and $\mathbf{G}_{\text{host}}(\mathbf{k}, \omega) = [\omega\sigma_0 - H_0]^{-1}$, while $\boldsymbol{\Sigma}^{(\text{int})}(\omega)$ is the interacting part (or proper) self-energy. With the non-interacting self-energy, the hybridization function can be written as,

$$\Gamma(\omega) = \frac{1}{2i} \iint \left[\boldsymbol{\Sigma}^{(0)}(\mathbf{k}, \omega - i\eta) - \boldsymbol{\Sigma}^{(0)}(\mathbf{k}, \omega + i\eta) \right] d^2k, \quad (6)$$

where $\eta \rightarrow 0$. The integration defined in Eq. (6) is highly peaked for small values of ω , therefore a high precision numerical integration is desirable to avoid numerical flaws. To achieve this purpose, we have used cubature rules as implemented in the Cuba package [29].

Note that $\Gamma(\omega)$ is also a 2×2 matrix and, in the presence of an external in-plane magnetic field, there is a spin-mixing rendering non-diagonal elements. To deal with the spin-mixing channels, a non-trivial Wilsonian RG chain is required [14]. As the hybridization matrix has, in general, non-zero off-diagonal complex elements, it is useful to decompose it in terms of Pauli matrices as, $\Gamma(\omega) = \sum_i d_i(\omega)\sigma_i$ ($i=0, x, y, z$). For convenience, we hereafter will rescale the bandwidth to unity ($D=1$), such that the relevant energy range is defined as $-1 < \omega < 1$, a standard procedure in impurity solvers. We also assume the impurity-altermagnet coupling to be $V=0.1$.

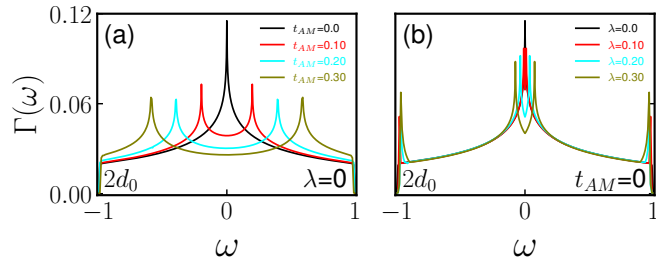


FIG. 3. Hybridization function $\hat{\Gamma}(\omega)$: (a) For $\lambda=0.0$ and $t_{AM} \neq 0$; (b) $t_{AM}=0.0$ and $\lambda \neq 0$. For both panels $\mathbf{B}=0$, and notice that we are showing the trace of $d_0\sigma_0$, as the diagonal terms are equal and there is no off-diagonal terms.

In Fig. 3 (a) and (b), we show $\Gamma(\omega)$ for different values of t_{AM} and λ , respectively, in absence of \mathbf{B} . Notice that regardless of the value of λ or t_{AM} , the diagonal terms for both panels are equal, as there is no spin-mixing terms in the hybridization matrix. Therefore, we only showed the trace of $d_0(\omega)\sigma_0 \propto 2d_0$, which is proportional to the total density of states. When t_{AM} is considered (with $\lambda=0$), one can observe a strong suppression of the peak around $\omega = 0$, with the development of a splitting. This suppression will be responsible to signatures in the Kondo temperature, as it will be discussed in the following section. For the case when RSOC is non-zero (with $t_{AM}=0$), shown in Fig. 3 (b), we can also notice a peak suppression similar to the Fig. 3 (a), however, the suppression is less pronounced, and there are peaks at the edge associated to the van Hove singularities. Since they are far away from the Fermi level, these van Hove singularities at the edges near the edge of conduction band is unimportant for the Kondo screening. The more pronounced suppression of the hybridization function near the Fermi level produced by t_{AM} anticipates the stronger suppression of Kondo screening caused by the altermagnet as compared to RSOC.

Now, we set the value of $t_{AM}=0.1$ and investigate how the presence of \mathbf{B} affects the hybridization matrix. In Fig. 4, we show $\Gamma(\omega)$ decomposed for different parameter configuration of \mathbf{B} and λ . In the absence of a magnetic field and RSOC ($\lambda=0$), d_0 is the only nonzero value as shown by the black solid line in Fig. 4 (a). However, notice that this result holds even for the case of $\lambda=0.2$ (dashed line). This behavior is because (i) the impurity is spin-independently coupled to the host, (ii) the AM

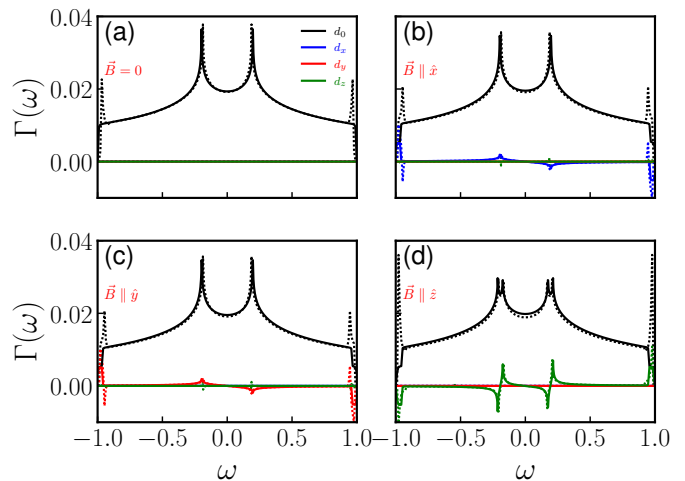


FIG. 4. Decomposition of the matrix hybridization function $\hat{\Gamma}(\omega)$ along different Pauli matrices σ_i with corresponding weights d_i . (a) For $\mathbf{B}=0$, (b) for a magnetic field along $\hat{\mathbf{x}}$, (c) for a magnetic field along $\hat{\mathbf{y}}$ and (d) for a magnetic field along $\hat{\mathbf{z}}$. The solid line is for $\lambda=0.0$, while the dashed line stands for $\lambda=0.2$. For panels (b)-(d), we have assumed $t_{AM} = 0.1$ and $B = 0.02$.

Hamiltonian [H_0 in Eq. (1)] preserves $C_{4z}\mathcal{T}$ symmetry and SOC is time-reversal invariant, rendering thus a diagonal and spin-independent $\Gamma(\omega)$. Nonetheless, notice that because $\lambda \neq 0$, we can still see the emergent peaks close to the edges of the conduction band associated to the appearance of van Hove singularities in the conduction band around the M -point. For an in-plane magnetic field Fig. 4 (b)-(c), the off-diagonal elements of $\hat{\Gamma}(\omega)$ will contribute to non-zero values for the coefficients d_y (d_x) for a magnetic field applied along x (y) conversely, while there is also a finite value for d_z that changes sign, i.e. $d_z \rightarrow -d_z$. Interestingly, for $\mathbf{B} \parallel \hat{\mathbf{z}}$ shown in Fig. 4 (d), the only nonzero components are along d_0 and d_z , even when $\lambda \neq 0$ (which intertwine the spin channels but does not break TRS). Furthermore, notice that because of the interplay between the AM exchange interaction and the Zeeman field, there is an enhancement of the d_z component, and also a marked *double* splitting in the peaks of d_0 , which will strongly reflect in the impurity spectral function.

III. INTERACTING REGIME AND KONDO SCREENING

Having obtained the hybridization function $\Gamma(\omega)$, we are ready to use the NRG method to address the Kondo effect in the system. This numerical technique is a powerful and standard impurity solver, which consists of a logarithmic discretization of the continuum conduction band in energy scales that decreases as $\Lambda^{-N/2}$, where Λ is a discretization parameter and N is the number of iterations in the NRG procedure. The discretized model is then mapped into a one-dimensional tight-binding-like Hamil-

tonian (aka Wilson chain Hamiltonian) whose length increase iteratively with N . The iterative diagonalization of a large- N Wilson chain is possible by proper truncation of Hilbert space at certain maximum dimension, allowing to access the energy around the Fermi level in a controllable manner [30]. Here, for practical purpose, we employ the NRG method to calculate the impurity retarded Green's function, from which we calculate the impurity density of states in the interacting regime. Within the Zubarev's notation [31], our Green's function can be written as

$$\mathcal{G}_{\text{imp}}^{\sigma\sigma'}(\omega) = \langle\langle d_{\sigma}; d_{\sigma'}^{\dagger} \rangle\rangle_{\omega}, \quad (7)$$

where $\langle\langle d_{\sigma}; d_{\sigma'}^{\dagger} \rangle\rangle_{\omega} = -i \int \Theta(t) \langle [d_{\sigma}(t), d_{\sigma'}^{\dagger}(0)]_+ \rangle e^{i\omega t} dt$. Here, $[d_{\sigma}(t), d_{\sigma'}^{\dagger}(0)]_+$ is the anti-commutator between the annihilation operator at time t with the creator operator at $t = 0$ at the impurity. The expectation value $\langle \cdot \rangle$ is taken in the ground state for zero temperature calculations.

The nontrivial energy dependence of the hybridization function requires an improved discretization scheme to reproduce with high resolution the initial function, thus reducing the numeric artifacts that can be present in the NRG calculations. To this end, we have used the adaptive “z-averaging” scheme [32] (with $N_z=5$), as implemented in the NRG Ljubljana open source code [33]. Furthermore, for the spectral functions calculations we have also used the self-energy “trick”, as described in [34] to remove nonphysical oscillations at the vicinity $\omega = 0$. For all the NRG calculations, we have assumed (unless stated otherwise) $\varepsilon_d = -U/2$ (particle-hole symmetry), $U=0.25$, $\Lambda=2$ and number of kept states = 2000.

A. Kondo temperature

We start by investigating the effect of the AM exchange field in the Kondo temperature of the system. The main quantity calculated here is the impurity density of state,

$$A_{\sigma}(\omega) = -\frac{1}{\pi} \text{Im}[\mathcal{G}_{\text{imp}}^{\sigma\sigma}(\omega)]. \quad (8)$$

It is known that $A(\omega) = \sum_{\sigma} A_{\sigma}(\omega)$ exhibits a many-body resonance at the Fermi level, known as Abrikosov-Shul resonance [35, 36] (or simply Kondo peak), as a signature of the Kondo screening [1]. This resonance not only signals the presence of Kondo screening in the system, but also provides a useful way to estimate T_K . Indeed, the width of the Kondo resonance can be directly associated to T_K [37–39]. In Fig. 5(a)-5(d) we make an insightful analysis on the behavior of T_K , extracted from the half-width at half-peak of the impurity spectral function, for different configurations of t_{AM} and λ , setting $\mathbf{B} = 0$. Fig. 5(a) shows $A(\omega)$ for different values of t_{AM} . For $t_{AM} = 0$ (black line), we see that $A(\omega)$ exhibits a split peak around $\omega = 0$. This splitting is induced by the sharp peak in the hybridization function $\Gamma(\omega)$ shown

in the Fig. 3(a) for $t_{AM} = 0$ (black curve). This splitting is analogous to the one observed in Ref. [40], resulting from an Anderson impurity coupled to a structured host density of states provided by a non-interacting energy level. Here, on the other hand, the sharp structure the conduction band is naturally provided by the van Hove singularity of the two-dimensional material. Now, as t_{AM} increases, we observe that Kondo peak evolves rapidly to a single and sharper peak, as already observed for $t_{AM} = 0.05$. This is because the sharp van Hove singularity is split for finite T_{AM} , leaving $\Gamma(\omega)$ relatively smooth near the Fermi level, as seen in Fig. 3(a) for finite t_{AM} . This prompt sharpening of the Kondo resonance, as t_{AM} increases reveals a strong dependence of T_K with t_{AM} . Fig. 5(c) shows how T_K decreases as t_{AM} increases as anticipated earlier in this paper.

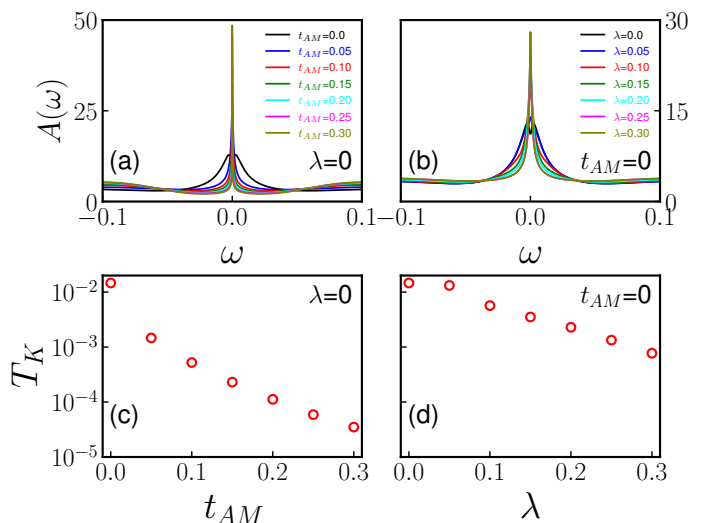


FIG. 5. (a) Impurity spectral function $A(\omega)$ for different values of t_{AM} with $\lambda=0$. (b) Impurity spectral function $A(\omega)$ for different values of λ with $t_{AM}=0$. (c) T_K as function of t_{AM} . (d) T_K as function of λ . For all panels, \mathbf{B} is set to zero.

To compare the effects of t_{AM} to λ on T_K , in Fig. 5(b) shows how $A(\omega)$ is affected the spin-orbit coupling λ . We now set $t_{AM} = 0$. We note that λ produces, qualitatively, a very similar to the effect of t_{AM} , although much less pronounced, as λ produces a very modest splitting of the $\Delta(\omega)$. Indeed, the effect of t_{AM} on T_K is much more important as compared to the effect of λ . By comparing Fig. 5(c) and Fig. 5(d) we observe that $t_{AM} = 0.3$ produces a suppression of T_K almost three order of magnitude, while for the same value of λ the suppression is about one order of magnitude.

Here, we should mention that the dependence of T_K with λ has been subject of interest over the past decades, and it is still source of debate in the literature [15]. For instance, Zarea et al. reported that away from the particle-hole symmetry in a 2DEG, the parity breaking Dzyaloshinsky-Moriya term is able to renormalize the antiferromagnetic Kondo coupling with an exponential enhancement of T_K [13]. A similar result has also been

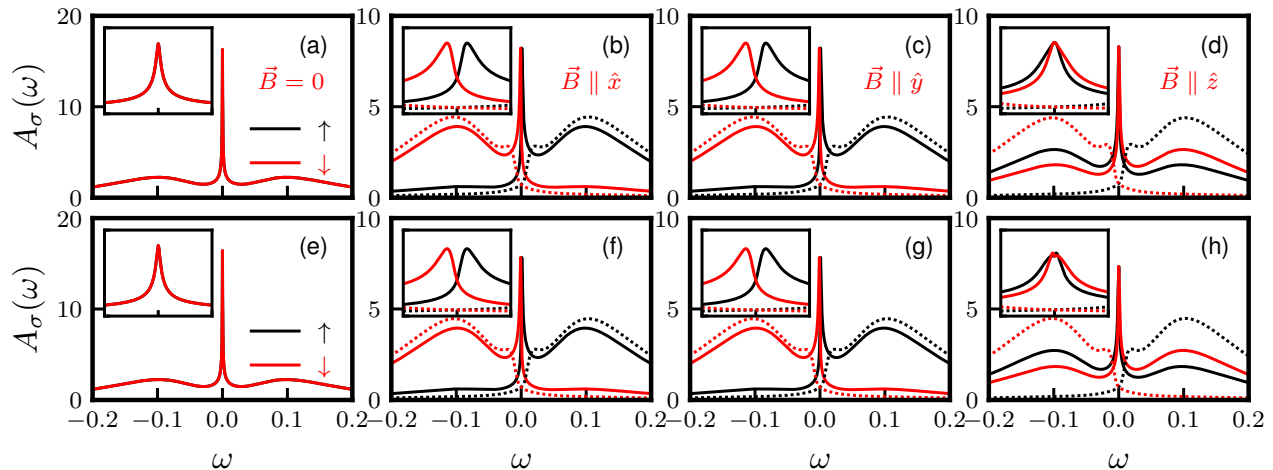


FIG. 6. Impurity spin-resolved local density of states $A_\sigma(\omega)$ projected along the direction of applied magnetic field \mathbf{B} . (a)-(d) for $\lambda = 0$ and $\mathbf{B} = 0, 0.002\hat{x}, 0.002\hat{y}, 0.002\hat{z}$, respectively. (e)-(h) are the same results, but for $\lambda = 0.2$. Solid lines (dashed) are for $g_{\text{imp}}=0.0$ ($g/g_{\text{imp}}=2.5$). The insets are zooms for the respective panel in the ω range $[-0.005, 0.005]$.

found by one of us for a quantum wire, even at the particle-hole symmetric point [41]. Interestingly, depending on how drastic is the modification of conduction band, we can also observe a suppression of T_K , as the RSOC is increased, as reported for a quantum wire in the absence of \mathbf{B} [14].

Within the NRG approach, it is quite clear that the change in the Kondo temperature is directly associated to the modification around the Fermi level in the density of states of the host material induced by properties of the band structure. Therefore, for a given fixed coupling V as in Eq. (4), enhanced density of the host material produces an enhancement of the T_K . A splitting of the Kondo peak is produced if $\rho(\omega)$ exhibit a peak at $\omega = 0$ whose width is similar or smaller than T_K . See for instance the discussion in Ref. [40].

B. Effect of magnetic field

In Sec. II, we have seen that the effect of magnetic field applied in the altermagnet is anisotropic. Therefore, anisotropic suppression of the Kondo should be observed. To see this, in Fig. 6 we show the spin-resolved local density of states (LDOS) at the impurity, $A_\sigma(\omega)$, for the magnetic field applied ($B = 0.02$) along different directions. We have set the g -factor ($g = 1$) for the host material (the altermagnet). The first and second rows show, respectively, results for $\lambda = 0.0$ and $\lambda = 0.2$ while solid and dashed lines corresponds to $g_{\text{imp}} = 0$ and $g_{\text{imp}} = 0.4g$, respectively.

Let us start looking the Fig. 6 (a) where there is no magnetic field applied, therefore all the projected component of A_σ are equal to each other. Interestingly, even though TRS is broken by AM exchange, because of the unusual spin splitting in momentum space, both spin-components of the \mathbf{G}_{host} contributes equally to the inte-

gral of Eq. 6. As expected, an inversion symmetry breaking induced by RSOC does not split $A_\sigma(\omega)$, as shown in Fig. 6 (e). Moreover, the results are almost unaffected when RSOC is included. Indeed, as observed in the insets of Fig. 6(a) and Fig. 6(b), the major splitting in the hybridization function is produced by t_{AM} .

Now, intriguing behavior occur when the magnetic field is considered. In Fig. 6(b)-(d) and Fig.6(f)-6(h) show LDOS projected along the different directions of applied \mathbf{B} . As such, for instance, if the magnetic field is applied along the x -direction, \uparrow and \downarrow refer to spin pointing towards positive and negating x -direction [42]. Having this in mind, we observe, that regardless the direction of the applied \mathbf{B} , a suppression of the Kondo peak accompanied by splitting of the Kondo peak. However, for an in-plane magnetic field, its interplay with the AM term and with \mathbf{B}_{SOC} brings a remarkable anisotropic effect in the LDOS as shown in Fig. 6(b)-6(c). Indeed, we see a stronger suppression of $A_\sigma(\omega)$ as compared to \mathbf{B} along the z -direction in Fig. 6(d) and (h). This anisotropic effect is observed only if the direct Zeeman effect is negligible in the impurity ($g_{\text{imp}} \approx 0$). If we consider $g_{\text{imp}} = 0.4$ as shown in dashed lines, the Kondo resonance peak is almost fully suppressed, as at this magnetic field strength both spins (band and impurity) are fully polarized, thus completely destroying the Kondo singlet state.

Before concluding, in Fig. 7 we show how the anisotropic magnetic response manifests in the total density of states, $A(\omega)$. To this end, we show $A(\omega)$ for different strengths and direction of the applied magnetic field. Upper and lower panels correspond to $g_{\text{imp}} = 0$ and $g_{\text{imp}} = 0.4g$. For $B = 0$ the Kondo peak can be clearly seen as shown in black line in Fig 7(a). Now, as \mathbf{B} increases the Kondo peak is progressively suppressed for magnetic field along either \hat{x} , \hat{y} and \hat{z} direction. As shown in Fig. 7(a) and 7(b) for $g_{\text{imp}}=0$. However, for field along z -direction the peak is less affected, as com-

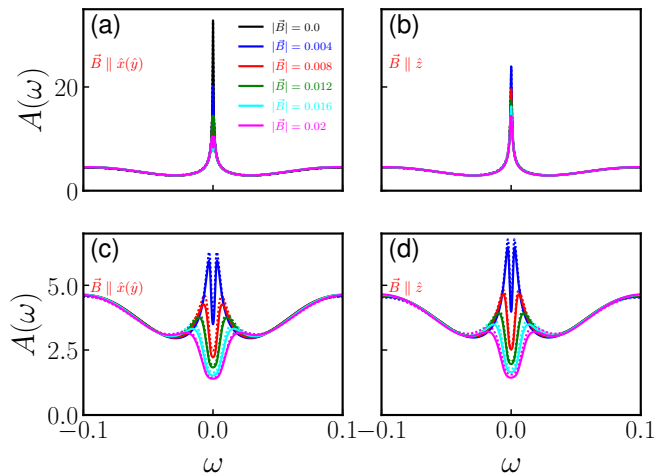


FIG. 7. Impurity local density of states $A(\omega) = \sum_{\sigma} A_{\sigma}(\omega)$ projected along the direction of applied magnetic field \mathbf{B} . (a) $A(\omega)$ along \hat{x} (or \hat{y} , by symmetry) for $g_{\text{imp}} = 0$ and $B = 0, 0.004, 0.008, 0.012, 0.016$ and 0.020 , respectively. (b) Same as in (a), but for $A(\omega)$ along \hat{z} . (c)-(d) are for $g/g_{\text{imp}} = 2.5$. Solid lines (dashed) are for $\lambda=0.0$ ($\lambda = 0.2$).

pared to the other directions. Again, this a signature of the anisotropic magnetic response of the system induced by the interplay between \mathbf{B} , AM and RSOC. Finally, for $g_{\text{imp}} = 0.4g$, the Kondo peak is strongly suppressed with an enhanced splitting, as shown in Fig. 7 (c)-(d), providing support that the system no longer sustain the Kondo single state.

IV. CONCLUSIONS

In summary, we have studied the Kondo screening effect in a spin-1/2 impurity coupled to a two-dimensional altermagnet in the presence of external magnetic field. By describing the system within a single-impurity Anderson Hamiltonian, we determined the hybridization func-

tion by exact calculation of the local Green's function, which allows us to garner the complete influence of the host material onto the impurity. We employ a numerical renormalization group approach to calculate the spin-resolved local density of states in the interacting regime, which allowed us to attain the low-temperature Kondo physics in the system. Our results shows a drastic decrease of the Kondo temperature T_K as the altermagnet coupling t_{AM} increases. By comparing this suppression with the one produced by the RSOC λ , we showed that the t_{AM} has a dominant effect in the suppression of T_K . Furthermore, despite the time-reversal symmetry broken by t_{AM} , it does not produce spin-splitting in the hybridization function. This is a direct consequence of the alternating momentum-dependent band spin-splitting that renders zero net magnetization to the impurity upon integration of the self-energy over the entire Brillouin zone. Moreover, we have investigated the effect of an applied magnetic field along different directions. The results showed an important anisotropic response of the system to the applied field. Indeed, a in-plane field has strong effect in Kondo screening marked by a sizable suppression of Kondo peak. In contrast, this suppression is less pronounced for a magnetic field along the z -direction. When the Zeeman coupling takes place directly in the impurity, the Kondo peak is overwhelmingly suppressed by the field and the anisotropic effect blurred. Our work shed light on the Kondo correlation in altermagnets and paves the way for future theoretical as well as experimental investigations of correlated phenomena in these materials.

ACKNOWLEDGMENTS

The authors acknowledge financial support from CAPES, FAPEMIG and CNPq. EV thanks FAPEMIG (Process PPM- 00631-17) and CNPq (Process 311366/2021-0). This work used resources of the ‘‘Centro Nacional de Processamento de Alto Desempenho em Sao Paulo (CENAPAD-SP).’’

-
- [1] A. C. Hewson, *The Kondo Problem to Heavy Fermions*, Cambridge Studies in Magnetism (Cambridge University Press, 1993).
- [2] J. Kondo, Resistance Minimum in Dilute Magnetic Alloys, *Progress of Theoretical Physics* **32**, 37 (1964).
- [3] W. De Haas and G. Van Den Berg, The electrical resistance of gold and silver at low temperatures, *Physica* **3**, 440 (1936).
- [4] Y. Jiang, P.-W. Lo, D. May, G. Li, G.-Y. Guo, F. B. Anders, T. Taniguchi, K. Watanabe, J. Mao, and E. Y. Andrei, Inducing kondo screening of vacancy magnetic moments in graphene with gating and local curvature, *Nature Communications* **9**, 2349 (2018).
- [5] A. Kurzmann, Y. Kleeorin, C. Tong, R. Garreis, A. Knothe, M. Eich, C. Mittag, C. Gold, F. K. de Vries, K. Watanabe, T. Taniguchi, V. Fal’ko, Y. Meir, T. Ihn, and K. Ensslin, Kondo effect and spin-orbit coupling in graphene quantum dots, *Nature Communications* **12**, 6004 (2021).
- [6] C. Piquard, P. Glidic, C. Han, A. Aassime, A. Cavanna, U. Gennser, Y. Meir, E. Sela, A. Anthore, and F. Pierre, Observing the universal screening of a kondo impurity, *Nature Communications* **14**, 7263 (2023).
- [7] P. Zalom, Rigorous wilsonian renormalization group for impurity models with a spectral gap, *Phys. Rev. B* **108**, 195123 (2023).
- [8] J. Martinek, Y. Utsumi, H. Imamura, J. Barnas, S. Maekawa, J. Konig, and G. Schon, Kondo effect in quantum dots coupled to ferromagnetic leads, *Phys. Rev. Lett.* **91**, 127203 (2003).
- [9] J. Martinek, M. Sindel, L. Borda, J. Barnas, J. Konig, G. Schon, and J. von Delft, Kondo effect in the presence

- of itinerant-electron ferromagnetism studied with the numerical renormalization group method, *Phys. Rev. Lett.* **91**, 247202 (2003).
- [10] A. N. Pasupathy, R. C. Bialczak, J. Martinek, J. E. Grose, L. A. K. Donev, P. L. McEuen, and D. C. Ralph, The kondo effect in the presence of ferromagnetism, *Science* **306**, 86 (2004), <https://www.science.org/doi/pdf/10.1126/science.1102068>.
- [11] R. Žitko and J. Bonča, Kondo effect in the presence of rashba spin-orbit interaction, *Phys. Rev. B* **84**, 193411 (2011).
- [12] A. Wong, S. E. Ulloa, N. Sandler, and K. Ingersent, Influence of rashba spin-orbit coupling on the kondo effect, *Phys. Rev. B* **93**, 075148 (2016).
- [13] M. Zarea, S. E. Ulloa, and N. Sandler, Enhancement of the kondo effect through rashba spin-orbit interactions, *Phys. Rev. Lett.* **108**, 046601 (2012).
- [14] E. Vernek, G. B. Martins, and R. Žitko, Anisotropic kondo screening induced by spin-orbit coupling in quantum wires, *Phys. Rev. B* **102**, 155114 (2020).
- [15] L. W. Smith, H.-B. Chen, C.-W. Chang, C.-W. Wu, S.-T. Lo, S.-H. Chao, I. Farrer, H. E. Beere, J. P. Griffiths, G. A. C. Jones, D. A. Ritchie, Y.-N. Chen, and T.-M. Chen, Electrically controllable kondo correlation in spin-orbit-coupled quantum point contacts, *Phys. Rev. Lett.* **128**, 027701 (2022).
- [16] I. Mazin (The PRX Editors), Editorial: Altermagnetism—a new punch line of fundamental magnetism, *Phys. Rev. X* **12**, 040002 (2022).
- [17] L. Šmejkal, J. Sinova, and T. Jungwirth, Emerging research landscape of altermagnetism, *Phys. Rev. X* **12**, 040501 (2022).
- [18] I. I. Mazin, K. Koepernik, M. D. Johannes, R. González-Hernández, and L. Šmejkal, Prediction of unconventional magnetism in doped FeSb_2 , *Proceedings of the National Academy of Sciences* **118**, e2108924118 (2021).
- [19] L. Šmejkal, A. B. Hellenes, R. González-Hernández, J. Sinova, and T. Jungwirth, Giant and tunneling magnetoresistance in unconventional collinear antiferromagnets with nonrelativistic spin-momentum coupling, *Phys. Rev. X* **12**, 011028 (2022).
- [20] M. Wei, L. Xiang, F. Xu, L. Zhang, G. Tang, and J. Wang, Gapless superconducting state and mirage gap in altermagnets (2023), [arXiv:2308.00248 \[cond-mat.supr-con\]](https://arxiv.org/abs/2308.00248).
- [21] Y. Zhu, T. Chen, Y. Li, L. Qiao, X. Ma, T. Hu, H. Gao, and W. Ren, Multipiezo effect in altermagnetic $v_2\text{seteo}$ monolayer (2023), [arXiv:2308.00234 \[cond-mat.mtrl-sci\]](https://arxiv.org/abs/2308.00234).
- [22] C. W. J. Beenakker and T. Vakhel, Phase-shifted andreev levels in an altermagnet josephson junction, *Phys. Rev. B* **108**, 075425 (2023).
- [23] S. A. A. Ghorashi, T. L. Hughes, and J. Cano, Altermagnetic routes to majorana modes in zero net magnetization (2023), [arXiv:2306.09413 \[cond-mat.mes-hall\]](https://arxiv.org/abs/2306.09413).
- [24] L. Šmejkal, A. Marmodoro, K.-H. Ahn, R. Gonzalez-Hernandez, I. Turek, S. Mankovsky, H. Ebert, S. W. D'Souza, O. Šipr, J. Sinova, and T. Jungwirth, Chiral magnons in altermagnetic RuO_2 (2022), [arXiv:2211.13806 \[cond-mat.mes-hall\]](https://arxiv.org/abs/2211.13806).
- [25] R. Bulla, T. A. Costi, and T. Pruschke, Numerical renormalization group method for quantum impurity systems, *Rev. Mod. Phys.* **80**, 395 (2008).
- [26] D. Zhu, Z.-Y. Zhuang, Z. Wu, and Z. Yan, Topological superconductivity in two-dimensional altermagnetic metals, *Phys. Rev. B* **108**, 184505 (2023).
- [27] This approximation can capture the essential physics of the system. however, a deeper analysis considering different orbitals and spin-dependent coupling between the impurity and the host might be relevant, specially for the microscopic description.
- [28] A. K. Mitchell and L. Fritz, Kondo effect in three-dimensional dirac and weyl systems, *Phys. Rev. B* **92**, 121109 (2015).
- [29] T. Hahn, Cuba—a library for multidimensional numerical integration, *Computer Physics Communications* **168**, 78 (2005).
- [30] K. G. Wilson, The renormalization group: Critical phenomena and the kondo problem, *Rev. Mod. Phys.* **47**, 773 (1975).
- [31] D. N. Zubarev, DOUBLE-TIME GREEN FUNCTIONS IN STATISTICAL PHYSICS, *Soviet Physics Uspekhi* **3**, 320 (1960).
- [32] R. Žitko and T. Pruschke, Energy resolution and discretization artifacts in the numerical renormalization group, *Phys. Rev. B* **79**, 085106 (2009).
- [33] R. Žitko, *Nrg ljubljana* (2021).
- [34] R. Bulla, A. C. Hewson, and T. Pruschke, Numerical renormalization group calculations for the self-energy of the impurity anderson model, *Journal of Physics: Condensed Matter* **10**, 8365 (1998).
- [35] P. Wiegmann, Towards an exact solution of the anderson model, *Physics Letters A* **80**, 163 (1980).
- [36] A. Tsvetick and P. Wiegmann, Exact results in the theory of magnetic alloys, *Advances in Physics* **32**, 453 (1983).
- [37] P. Nozieres, A fermi-liquid description of the kondo problem at low temperatures, *Journal of Low Temperature Physics* **17**, 31 (1974).
- [38] A. C. Hewson, Renormalized perturbation expansions and fermi liquid theory, *Phys. Rev. Lett.* **70**, 4007 (1993).
- [39] D. Jacob, Temperature evolution of the kondo peak beyond fermi liquid theory, *Phys. Rev. B* **108**, L161109 (2023).
- [40] L. G. G. V. Dias da Silva, N. P. Sandler, K. Ingersent, and S. E. Ulloa, Zero-field kondo splitting and quantum-critical transition in double quantum dots, *Phys. Rev. Lett.* **97**, 096603 (2006).
- [41] G. R. de Sousa, J. F. Silva, and E. Vernek, Kondo effect in a quantum wire with spin-orbit coupling, *Phys. Rev. B* **94**, 125115 (2016).
- [42] To obtain the LDOS projected along different spin directions we calculate the corresponding Green's function, which can be obtained by combining appropriately the components given by Eq. (7).